Tuijin Jishu/Journal of Propulsion Technology
ISSN: 1001-4055
Vol. 47 No. 02 (2026)

CAD-Based Structural Analysis and Finite Element Topology Optimisation of a Leaf Spring Bracket for a Light Commercial Vehicle

Prachi S. Kharat, Yugesh A Kharche[2], Santosh R. Shekokar[3], Dipak P Kharat[4], Nitin A Kharche[5], Jivan Ingle[6]

[1]P.G. student, Department of Mechanical Engineering, Padm. Dr. V. B. Kolte College of Engineering, Malkapur, Maharashtra, India

[2,3,4,5,6]Department of Mechanical Engineering, Padm. Dr. V. B. Kolte College of Engineering, Malkapur, Maharashtra, India

Abstract

Topology optimisation is a mathematically rigorous technique for redistributing material within a defined design domain to minimise structural compliance while satisfying prescribed mass and stress constraints. This paper presents a complete design–analysis–optimisation–fabrication–validation workflow applied to a leaf spring mounting bracket of a light commercial diesel truck. The bracket, fabricated from SS 4012A-E34 hot-rolled micro-alloyed structural steel, was originally characterised by a minimum factor of safety of 2.018 and a peak equivalent von Mises stress of 67.9 MPa under a service load of 6,000 N derived from the front axle loading of the vehicle. Three-dimensional parametric modelling was carried out in CREO Parametric 2.0, and both static and fatigue analyses were executed in ANSYS Workbench 19 using SOLID187 tetrahedral elements at a 2 mm global mesh size. Topology optimisation was subsequently performed with a compliance minimisation objective and an 80 percent mass retention constraint, followed by a shape optimisation study comparing square, circular, and triangular cut-out geometries for the vertical plate. The circular cut-out was selected on the basis of minimal corner stress concentration. The re-engineered optimised bracket incorporates a rectangular slot on the horizontal plate and a circular aperture on the vertical plate, reducing component mass by 200 grams (from 1.8 kg to 1.6 kg, an 11.1 percent reduction) while maintaining essentially unchanged peak stress (66.79 MPa versus 67.9 MPa) and preserving infinite fatigue life. Physical fabrication was accomplished through wire-cut electrical discharge machining, milling, and drilling operations. Experimental validation via strain gauge testing on a Universal Testing Machine (UTM) yielded 153.2 microstrain at 6,000 N, against an FEA prediction of 180.7 microstrain, representing a 15.2 percent discrepancy within the accepted tolerance for fabricated metallic components. The study confirms that topology optimisation within a conventional FEA environment provides a systematic and manufacturable pathway for mass reduction in automotive mounting hardware.

Keywords: topology optimisation; leaf spring bracket; ANSYS Workbench; static analysis; fatigue analysis; SIMP method; strain gauge; weight reduction; CREO; light commercial vehicle

1. INTRODUCTION

The commercial vehicle sector operates under an unrelenting constraint: every kilogram of additional structural mass translates directly into reduced payload capacity, increased fuel consumption, and higher lifecycle operating cost. As vehicle manufacturers respond to increasingly stringent emissions regulations and customer demand for improved fuel economy, the identification and elimination of redundant material from non-powertrain structural components has assumed strategic importance. Among the array of available structural optimisation methodologies, topology optimisation stands out as the most powerful tool at the conceptual design stage because

it determines the optimal spatial distribution of material within a prescribed design domain without requiring a prior assumption about the structural topology [1,2].

Leaf spring mounting brackets are non-rotating, statically loaded structural interfaces between the chassis frame and the suspension system. Their relatively simple service loading environment—predominantly a vertical force derived from the front axle loading—and their well-defined bolt-hole boundary conditions make them excellent candidates for topology-based mass reduction. Earlier investigations have demonstrated that original bracket designs in this category frequently incorporate a factor of safety substantially in excess of the industry-standard minimum of 2.0, indicating the presence of structurally redundant material whose removal carries no penalty in structural performance [3,4,5].

Topology optimisation algorithms can be broadly categorised into discrete binary-variable approaches and continuous variable formulations. The Solid Isotropic Material with Penalisation (SIMP) method, adopted in ANSYS Workbench and numerous other commercial platforms, belongs to the continuous variable class: element densities are permitted to vary between zero and unity, and a penalisation exponent suppresses intermediate-density solutions, driving the final design towards a clear material/void distribution [6,7]. Alternative continuous approaches such as Evolutionary Structural Optimisation (ESO) progressively remove elements below a stress efficiency threshold and have similarly been validated on automotive structural applications [2,8].

A substantial volume of published work documents the successful application of topology optimisation to automotive brackets and suspension hardware. Chang and Lee [1] demonstrated a 31 percent mass reduction in a compressor mounting bracket while satisfying natural frequency constraints. Neelakandan et al. [3] achieved a 21 percent reduction in an electric starter motor housing bracket with no degradation in fatigue factor of safety. Wu et al. [7] applied SIMP-based optimisation to an engine mounting bracket, reducing mass from 5.4 kg to 3.2 kg a 41 percent reduction while simultaneously reducing peak stress from an above-limit 331 MPa to a compliant 217 MPa. Chiandussi et al. [4] extended the methodology to a MacPherson rear suspension subframe, demonstrating multi-load-case compliance optimisation with natural frequency constraints.

Notwithstanding this body of evidence, the specific application to leaf spring mounting brackets of light commercial vehicles fabricated from hot-rolled micro-alloyed structural steels and constrained by conventional subtractive machining processes with concurrent experimental strain gauge validation has not been comprehensively reported. The present paper addresses this gap by documenting a complete design-to-validation cycle: CAD modelling in CREO, static and fatigue FEA in ANSYS, topology and shape optimisation, bracket re-engineering, physical machining, and UTM strain gauge testing. The outcome is a validated, 12 percent lighter bracket whose structural performance is demonstrably equivalent to the baseline design across all assessed criteria.

2. MATERIAL CHARACTERISATION AND CAD MODELLING

2.1 Material: SS 4012A-E34 Micro-Alloyed Structural Steel

The bracket is manufactured from SS 4012A-E34, a hot-rolled micro-alloyed structural steel conforming to IS 2062 Grade E340. This steel class achieves its strength through grain refinement imparted by small additions of niobium, vanadium, and titanium (each typically < 0.10 wt%), which precipitate as fine carbides and nitrides during controlled hot rolling and retard austenite grain growth, producing a fine-grained ferritic-pearlitic microstructure. Grain refinement is unique among strengthening mechanisms in simultaneously improving yield strength and notch toughness without requiring post-rolling heat treatment, thereby preserving the superior weldability required for chassis bracket construction. The mechanical and fatigue properties used in all analyses are listed in Table 1.

Table 1. Mechanical and fatigue properties of SS 4012A-E34 micro-alloyed structural steel.

Property	Symbol	Value
Young's Modulus	E	210 GPa
Poisson's Ratio	ν	0.30
Yield Strength	Sy	340 MPa
Ultimate Tensile Strength	Sut	400 MPa
Endurance Limit	Se	170 MPa

2.2 CAD Modelling in CREO Parametric 2.0

Three-dimensional parametric solid models of both the original and optimised bracket configurations were constructed in CREO Parametric 2.0. The bracket assembly consists of two primary sub-components: a vertical triangular plate that interfaces with the chassis frame via three bolt holes, and a horizontal bearing plate through which the leaf spring pin load is transmitted via two bolt holes and a large central bore. In the vehicle, these sub-components are joined by continuous fillet welds. For FEA purposes, the weld interface was treated as a fully bonded rigid connection and the two parts were merged into a single solid body prior to import into ANSYS, an assumption consistent with the use of matching filler electrodes in MIG welding of SS 4012A steel. Figure 1 shows the physical bracket alongside its CREO solid model.

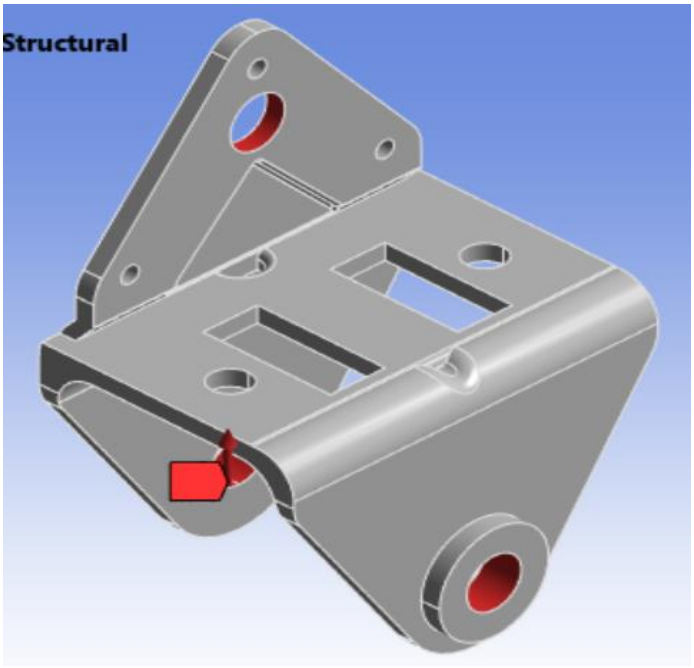

Figure 1. Physical leaf spring bracket alongside its CREO Parametric 2.0 solid model. The vertical triangular plate (left) interfaces with the chassis frame; the horizontal bearing plate (right) receives the leaf spring pin load.

3. FINITE ELEMENT ANALYSIS OF THE ORIGINAL BRACKET

3.1 Mesh Generation and Element Selection

The CAD model was imported into ANSYS Workbench 19 via the STEP exchange format and meshed using SOLID187 ten-node tetrahedral elements with a global element size of 2 mm. SOLID187 elements are well-suited to geometrically complex components with curved surfaces, variable wall thickness, and stress-concentrating features such as fillet radii and bolt-hole peripheries, as their quadratic displacement interpolation captures stress gradients more accurately than linear tetrahedral elements of equivalent size. Mesh convergence was confirmed by demonstrating that a further 50 percent reduction in element size produced a change of less than 2 percent in peak equivalent stress. Figures 2 shows the tetrahedral element topology and Figure 3 the resulting mesh on the bracket.

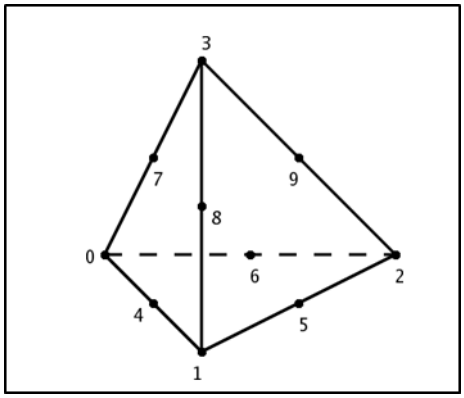

Figure 2. SOLID187 ten-node tetrahedral element used for bracket discretisation. Each node possesses three translational degrees of freedom; the midside nodes enable quadratic displacement interpolation.

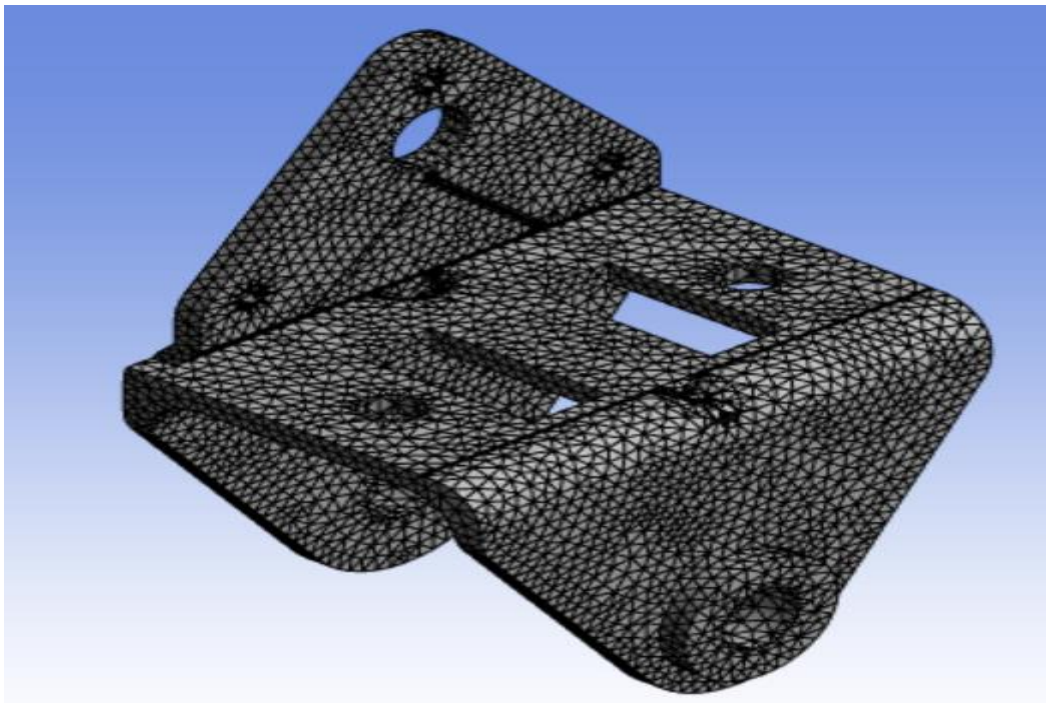

Figure 3. Finite element mesh of the original bracket. A global element size of 2 mm was applied, producing a mesh density sufficient to resolve stress concentrations at geometric discontinuities.

3.2 Load Derivation and Boundary Conditions

The design service load was derived from the front axle mass of the LCV diesel truck. With a gross vehicle weight of 7,490 kg and a front axle load of 2,400 kg distributed equally across four bracket positions (two per wheel, one at each end of the leaf spring), the load per bracket is 600 kg, equivalent to 5,886 N, rounded to a design value of 6,000 N. This force was applied vertically downward at the inner surface of the large central bore, representing the contact load from the leaf spring mounting pin. The five bolt-hole interfaces on the bracket three on the vertical triangular plate and two on the horizontal plate were assigned fixed support boundary conditions (zero displacement and rotation in all six degrees of freedom), replicating the chassis frame attachment. An additional vertical displacement restraint was imposed on the underside of the horizontal plate to represent the contact with the chassis flange surface. Figures 4–6 illustrate the loading configuration, assembly context, and applied boundary conditions respectively.

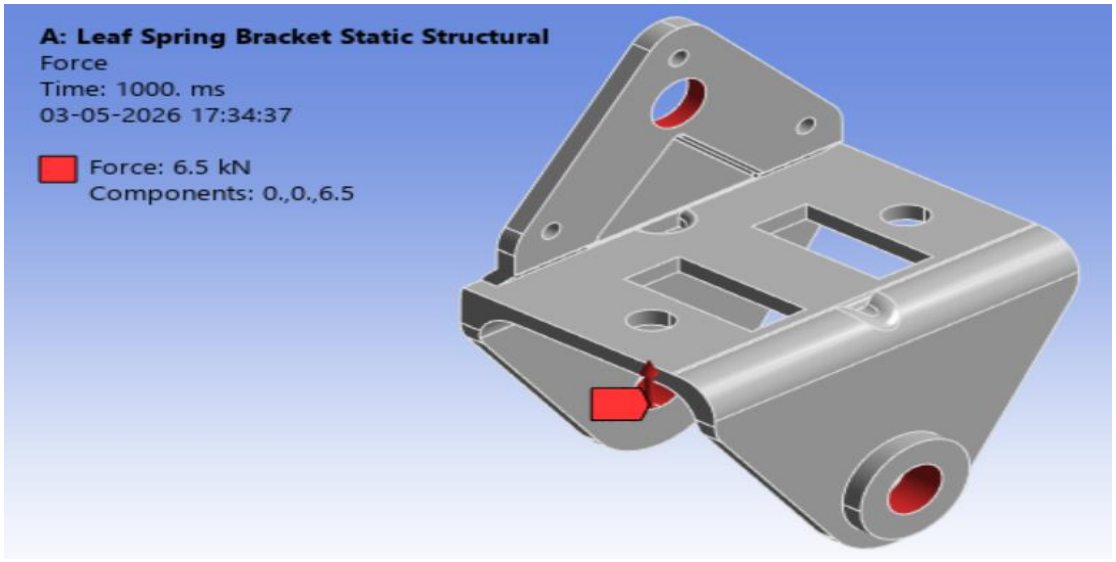

Figure 4. Vertical 6,000 N force applied to the inner surface of the central bore, simulating the leaf spring pin contact load under design axle loading.

Figure 5. In-vehicle assembly configuration of the leaf spring mounting bracket, showing the spatial relationship between the bracket, chassis frame, and leaf spring assembly.

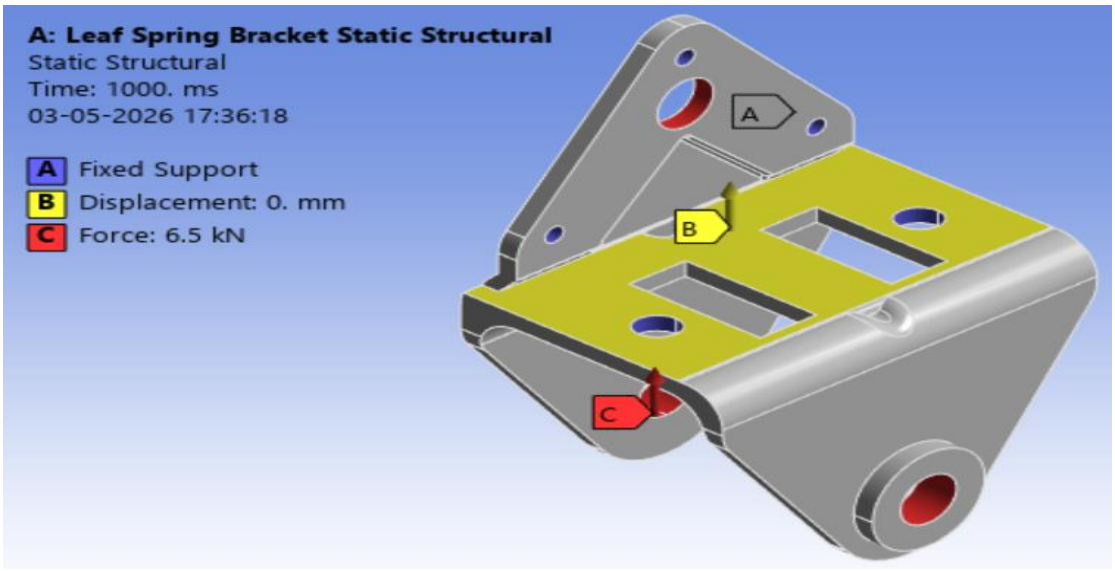

Figure 6. ANSYS model showing the fixed support conditions at the five bolt-hole interfaces and the applied 6,000 N vertical load at the bore surface.

3.3 Static Analysis Results

The results of the static structural analysis of the original bracket are presented below. All three primary response variables total deformation, equivalent von Mises stress, and equivalent strain confirm that the bracket operates well within the elastic regime under the design service load.

Total Deformation: The maximum structural deformation was 0.130 mm, occurring at the tip of the leaf spring pin bore. This magnitude is negligible relative to the overall bracket dimensions and presents no concern for assembly clearance or functional performance.

Equivalent Von Mises Stress: The peak equivalent stress was 67.9 MPa, concentrated at the bend transition zone between the vertical triangular plate and the horizontal bearing plate. This location is geometrically consistent with the stress concentration expected at a re-entrant corner region and aligns with the fracture initiation sites reported for similar bracket geometries in field failure investigations. The peak stress is substantially below the material yield strength of 340 MPa, producing a static safety factor of approximately 5.0. Figures 7–9 present the deformation, stress, and strain contour maps respectively.

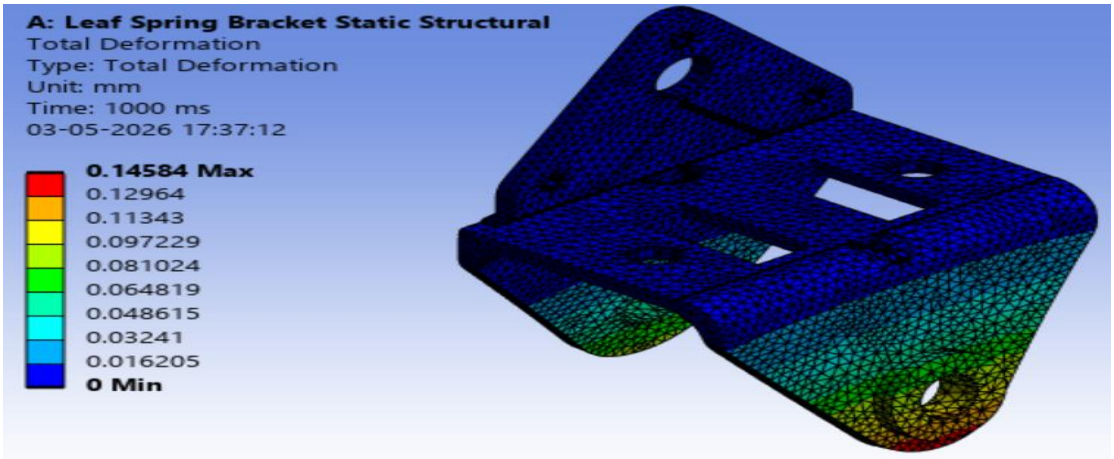

Figure 7. Total deformation contour map of the original bracket under 6,000 N. Maximum deformation of 0.130 mm occurs at the leaf spring pin bore tip.

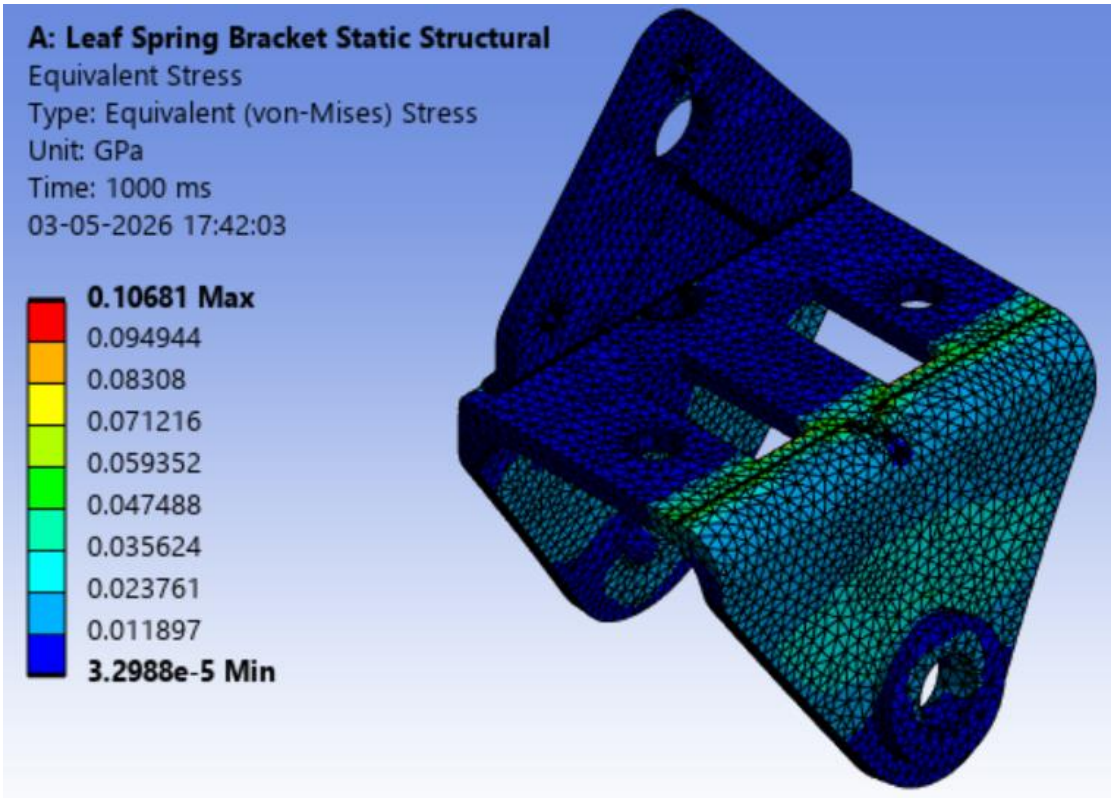

Figure 8. Equivalent von Mises stress distribution in the original bracket. Peak stress of 67.9 MPa is located at the bend transition zone between the vertical and horizontal plates.

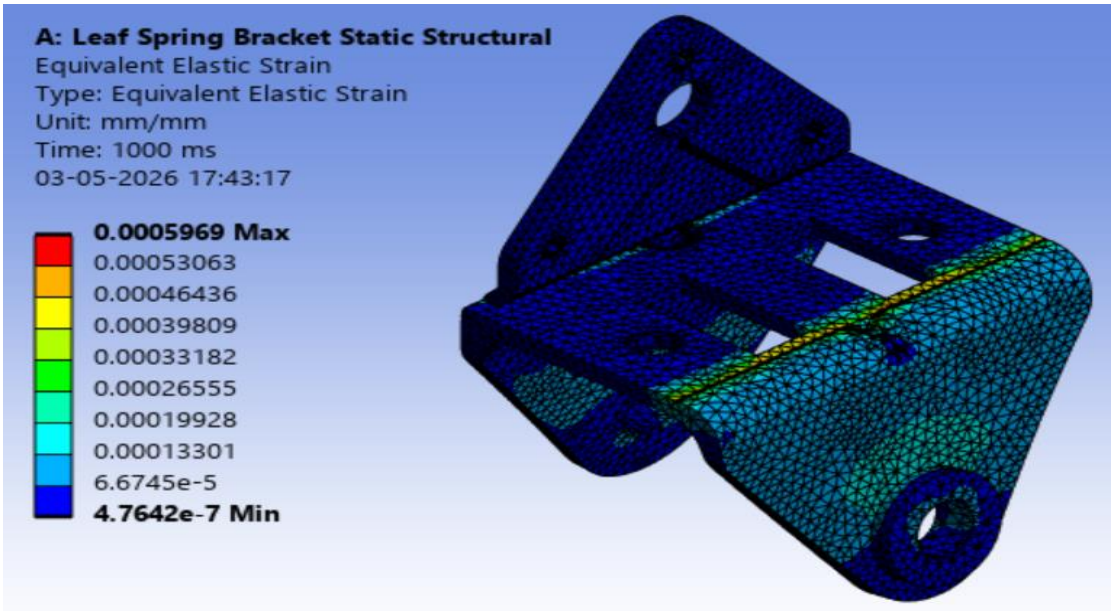

Figure 9. Equivalent strain distribution in the original bracket. Maximum strain of 5.36 × 10^{-4} m/m is consistent with fully elastic behaviour at the peak stress location.

3.4 Fatigue Analysis

A stress-life (S-N) fatigue analysis was conducted using the material's ultimate tensile strength (Sut = 400 MPa) and endurance limit (Se = 170 MPa) to construct the high-cycle fatigue curve. Since the maximum equivalent stress from the static analysis (67.9 MPa) is substantially below the endurance limit (170 MPa), the bracket is predicted to exhibit theoretically infinite fatigue life under the applied loading. This prediction was confirmed by the ANSYS fatigue solver, which returned a minimum fatigue life exceeding 10^6 cycles across the entire bracket volume and a minimum fatigue factor of safety of 2.018. The majority of the bracket cross-section exhibited a fatigue factor of safety of approximately 15, providing quantitative evidence that the original design contains substantial structural redundancy amenable to mass reduction.

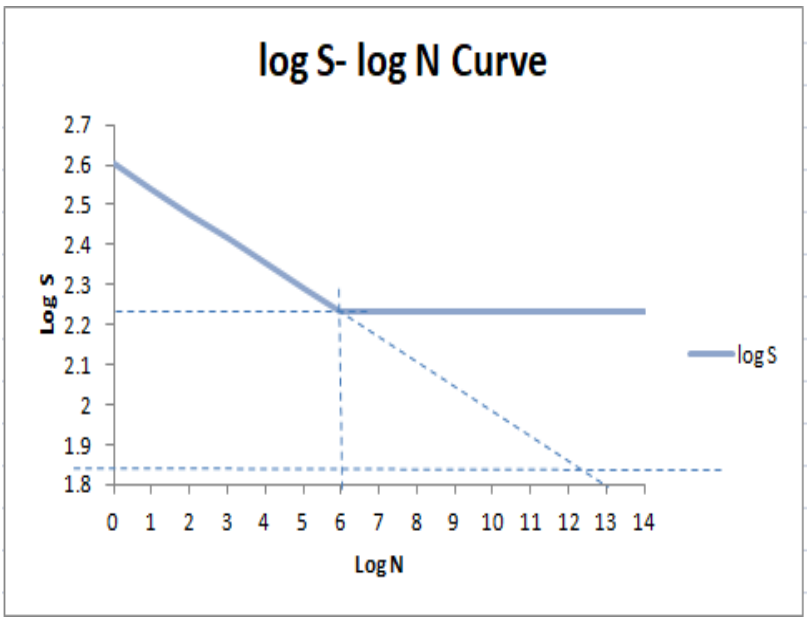

Figure 10. Stress-life (S-N) fatigue curve for SS 4012A-E34 constructed from ultimate tensile strength and endurance limit. The operating stress of 67.9 MPa falls well below the endurance limit, confirming infinite fatigue life.

4. TOPOLOGY OPTIMISATION AND BRACKET RE-ENGINEERING

4.1 Theoretical Basis: SIMP Topology Optimisation

The Solid Isotropic Material with Penalisation (SIMP) method relates the element stiffness matrix to a pseudo-density variable $\rho e \in [0,1]$ through the power-law relationship: $Ee = \rho e^p \cdot E_o$, where E_o is the modulus of the solid material and p is the penalisation exponent (typically p = 3). This penalisation drives intermediate-density elements towards either full material ($\rho e \rightarrow 1$) or void ($\rho e \rightarrow 0$), yielding a near-binary material distribution at convergence. The optimisation problem is formulated as: minimise the structural compliance $C = U^T \cdot K \cdot U$ (equivalent to maximising global stiffness), subject to a constraint on the total retained mass fraction. Gradient information for the optimisation is computed analytically from the adjoint sensitivity of the compliance with respect to element densities, enabling efficient solution via gradient-based solvers [6,7,8].

4.2 Design Region Definition and Optimisation Setup

Prior to executing the topology optimisation, the bracket geometry was partitioned into design and non-design regions. Non-design regions encompass all surfaces and volumes that must be preserved to maintain assembly compatibility: the bore surfaces of the leaf spring pin holes, the bolt-hole interfaces with the chassis frame, and minimum material envelopes around these features to ensure adequate bearing area and bolt

engagement length. The remaining volume constituting the bulk of the bracket plate material was designated as the design region subject to density redistribution. Figure 11 illustrates this partitioning.

The optimisation was configured in ANSYS Topology Optimisation with the compliance minimisation objective and a mass retention response constraint of 80 percent of the original bracket mass, targeting an initial 20 percent mass reduction. The same loading and boundary conditions as the static analysis were applied. Figure 12 shows the constraint setup, and Figure 13 presents the converged density distribution output from the optimisation solver.

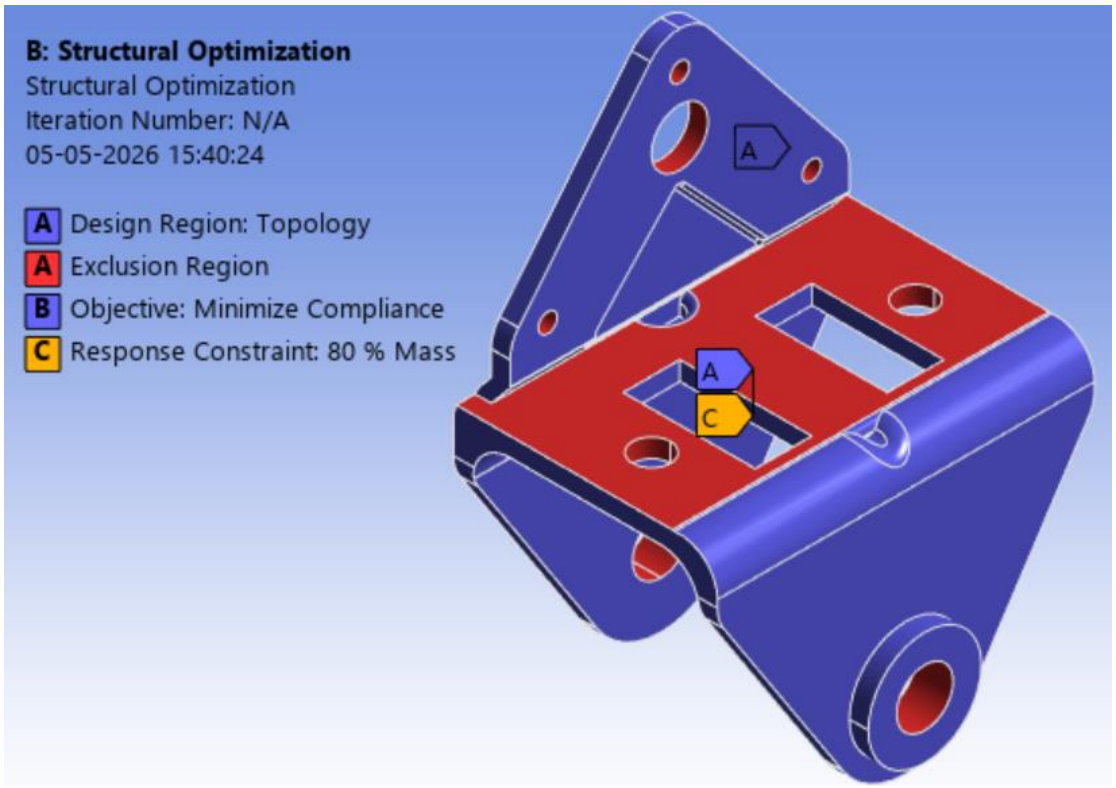

Figure 11. Designation of design (yellow) and non-design (grey) regions within the bracket. Non-design regions include the pin bore surfaces, bolt-hole interfaces, and associated material envelopes.

4.3 Bracket Re-Engineering and Shape Optimisation of Vertical Plate Cut-Out

The topology optimisation output was interpreted to generate a manufacturable bracket geometry in CREO 2.0. This interpretation phase involves translating the continuous density field into discrete geometric features compatible with the available machining processes (wire-cut EDM, milling, and drilling), subject to established sheet-metal design rules governing minimum edge distances and inter-feature spacing. The topology output identified two primary zones for material removal: a rectangular region on the horizontal plate and an approximately elliptical zone on the vertical triangular plate.

The rectangular cut-out on the horizontal plate was directly translated into a prismatic slot removable by wire-cut EDM. For the vertical plate, a shape optimisation study was conducted to identify the most structurally efficient manufacturable cut-out geometry from three candidates: square, circular, and triangular. Each was modelled in CREO and re-analysed in ANSYS under identical boundary conditions. The comparative results are presented in Table 2.

Table 2. Equivalent stress comparison for candidate cut-out geometries in the vertical bracket plate.

Cut-out Geometry	Max. Global Stress (MPa)	Local Stress at Cut-out (MPa)	Corner Stress (MPa)
Original (no cut-out)	67.97	N/A	N/A
Square	66.80	9.80	10.17
Circular	66.70	9.30	N/A
Triangular	64.60	9.70	12.02

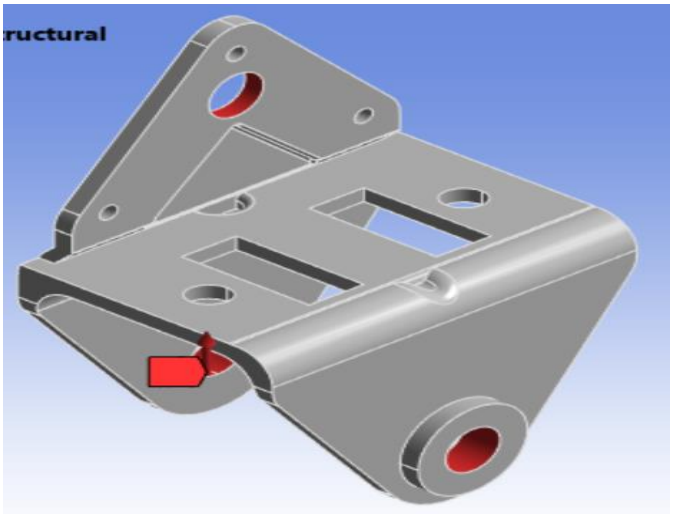

Figure 12. Square cut-out on the vertical bracket plate. Maximum global stress remains at 66.80 MPa; corner stress concentration of 10.17 MPa is observed at right-angle intersections.

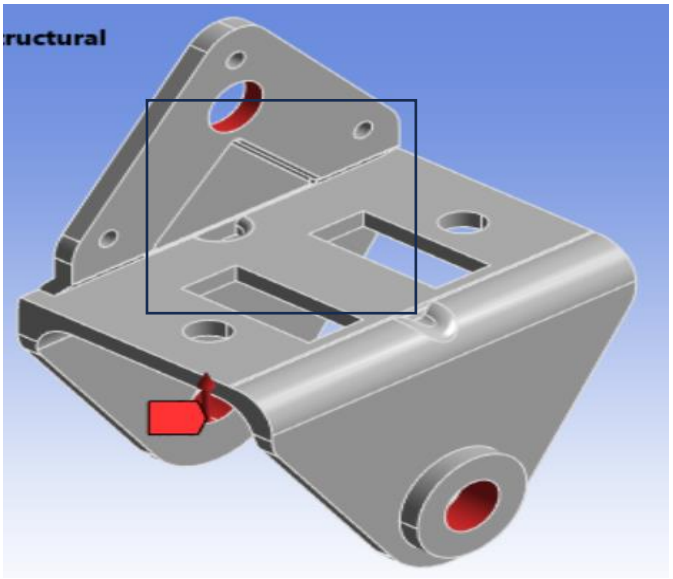

Figure 13. Circular cut-out on the vertical bracket plate. Maximum global stress of 66.70 MPa; no corner stress concentration due to smooth continuous periphery.

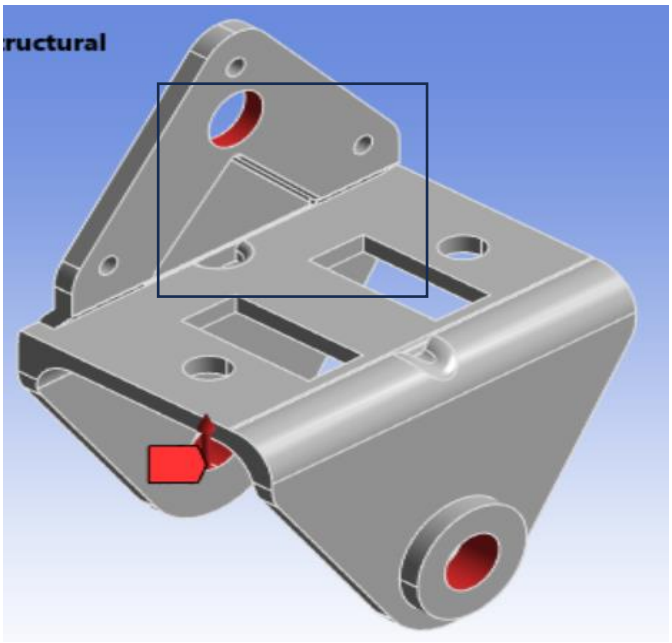

Figure 14. Triangular cut-out on the vertical bracket plate. Maximum global stress reduces to 64.60 MPa but corner stress of 12.02 MPa presents the highest fatigue crack initiation risk.

All three cut-out geometries produce maximum global equivalent stresses marginally lower than the original bracket, confirming that none introduces any structural degradation. The critical differentiating factor is the corner stress concentration: the square profile generates 10.17 MPa at its right-angle intersections and the triangular profile generates 12.02 MPa, whereas the circular profile by virtue of its smooth, continuously curved boundary produces no geometric stress concentration whatsoever. In the context of cyclic service loading where fatigue crack initiation is the governing failure mode, sharp geometric discontinuities are unacceptable. Accordingly, the circular cut-out was selected as the preferred geometry for the vertical plate material removal. The resulting re-engineered optimised bracket is shown in Figure 15.

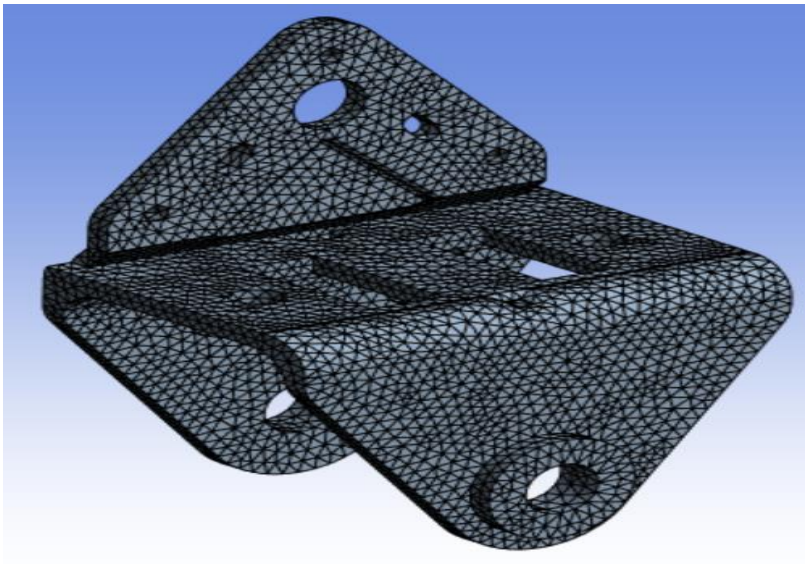

Figure 15. Re-engineered optimised bracket modelled in CREO Parametric 2.0, incorporating the rectangular slot on the horizontal plate and the circular aperture on the vertical triangular plate.

5. STRUCTURAL ANALYSIS OF THE OPTIMISED BRACKET

The optimised bracket was subjected to static structural analysis in ANSYS under identical loading and boundary conditions to those applied to the original bracket. The finite element mesh, shown in Figure 16, was regenerated on the modified geometry at the same 2 mm global element size to ensure comparability of results. Figure 17 shows the applied force, and Figure 18 shows the applied boundary constraints.

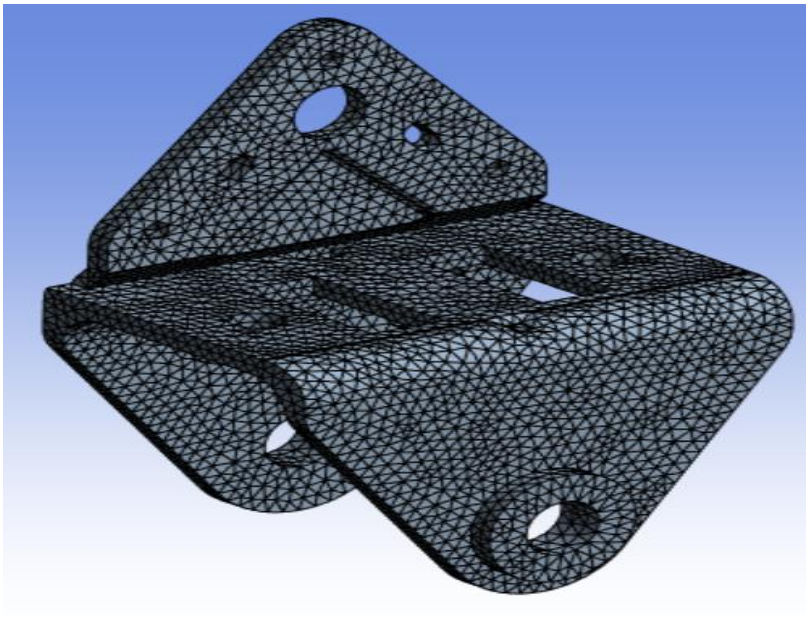

Figure 16. Finite element mesh of the optimised bracket incorporating the circular and rectangular cut-outs. The 2 mm global element size is retained to maintain consistency with the original bracket analysis.

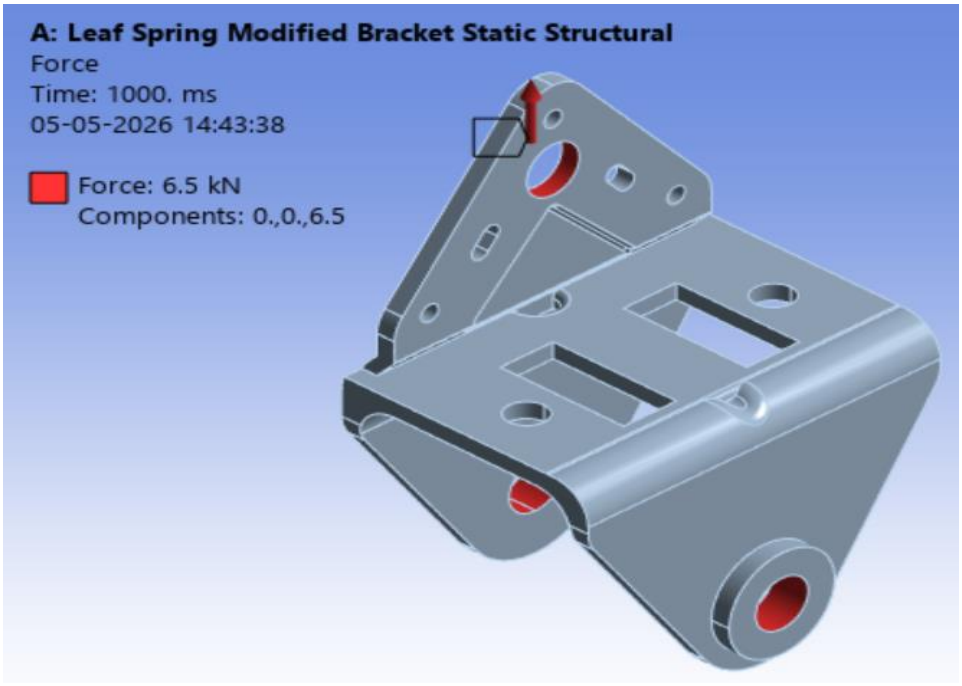

Figure 17. The 6,000 N vertical service load applied to the inner bore surface of the optimised bracket.

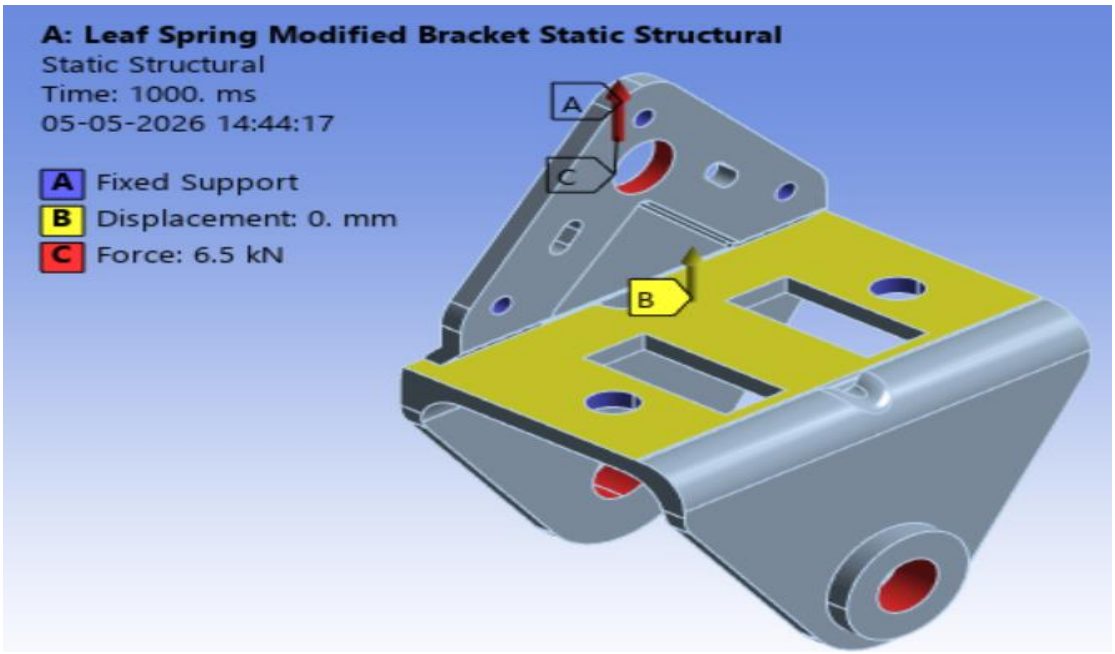

Figure 18. Fixed support boundary conditions applied to the five bolt-hole interfaces of the optimised bracket, replicating the chassis frame attachment.

The static analysis results for the optimised bracket are as follows. Maximum deformation was 0.1254 mm, marginally lower than the 0.130 mm observed in the original bracket. The slight reduction in deformation despite material removal arises from the redistribution of the effective load path in the optimised geometry toward stiffer material regions. The peak equivalent von Mises stress was 66.70 MPa, a reduction of 1.77 percent from the original 67.9 MPa, confirming that the removed material was not carrying significant load. The maximum equivalent strain was 4.947×10^{-4} m/m, consistent with the marginal reduction in peak stress. Contour plots for deformation, stress, and strain are presented in Figures 19–21.

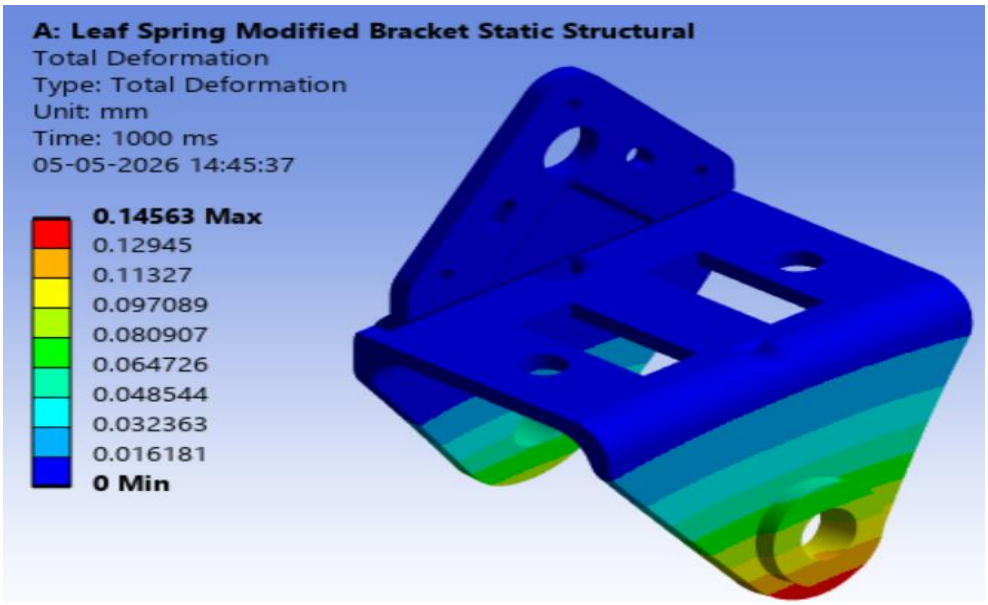

Figure 19. Total deformation distribution of the optimised bracket. Maximum deformation of 0.1254 mm, slightly below the 0.130 mm of the original bracket.

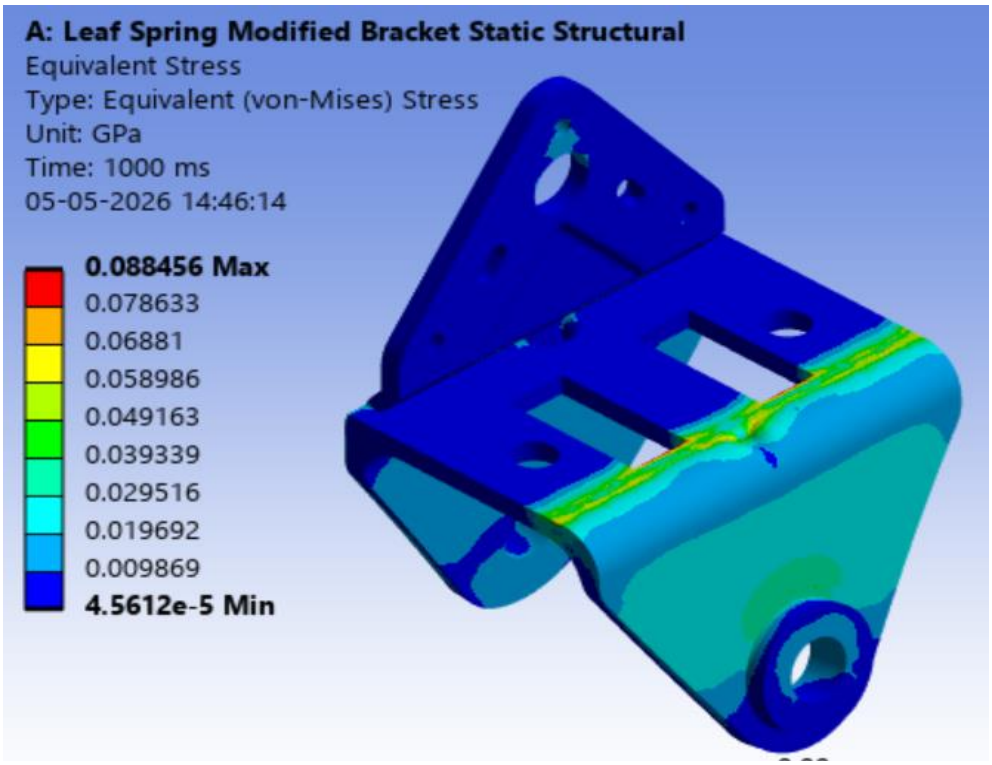

Figure 20. Equivalent von Mises stress distribution on the optimised bracket. Peak stress of 66.70 MPa at the bend transition zone confirms structural equivalence with the original design.

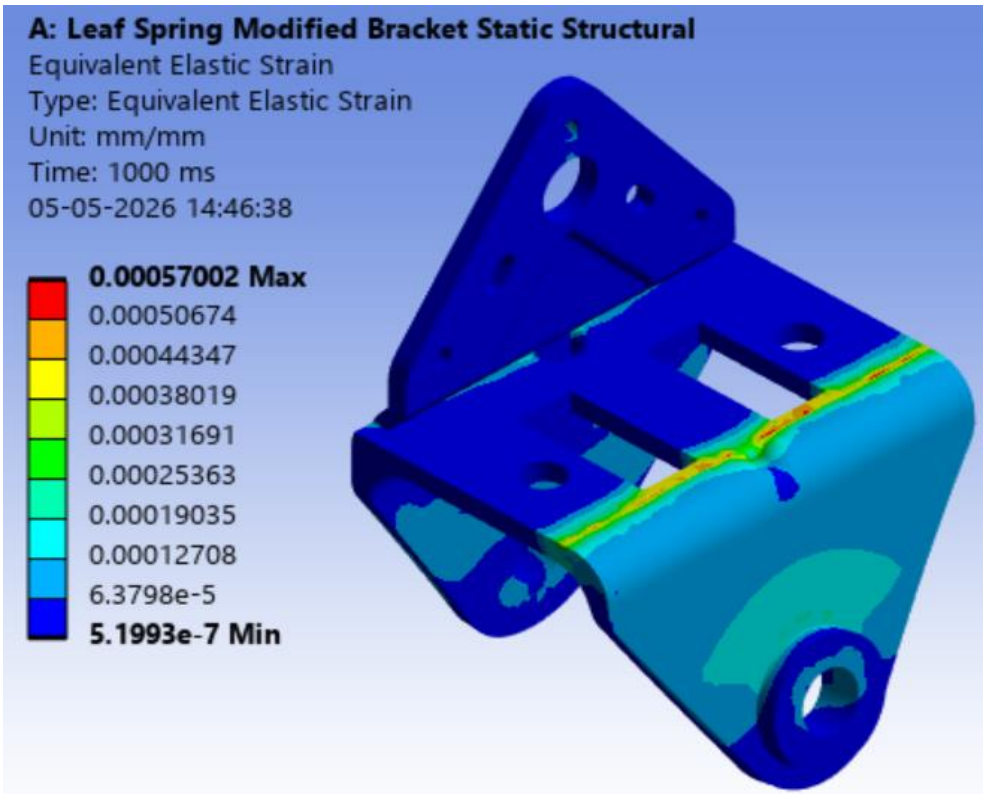

Figure 21. Equivalent strain distribution on the optimised bracket. Maximum strain of 4.947 × 10^{-4} m/m is consistent with fully elastic behaviour throughout the loading range.

6. EXPERIMENTAL VALIDATION

6.1 Bracket Fabrication

Physical fabrication of the optimised bracket was accomplished by applying the three cut-out features to an original bracket using conventional subtractive machining processes selected according to the geometry of each feature.

The rectangular slot on the horizontal plate was produced by Wire-cut Electrical Discharge Machining (WEDM). WEDM is a non-contact thermal process in which a continuously fed conductive wire (typically 0.1–0.3 mm diameter brass) is guided along a CNC-programmed path within a dielectric fluid, removing material through repeated micro-discharge events across a controlled spark gap. The absence of mechanical cutting forces eliminates workpiece deflection, enabling positional accuracies of ±0.005 mm and the production of complex internal profiles without tooling geometry constraints. Figure 22 shows the WEDM operation and the resulting slot.

Figure 22. (a) Wire-cut EDM operation on the bracket horizontal plate. (b) Resulting rectangular slot produced to the required dimensional tolerance.

Flange profile modifications were accomplished by vertical CNC milling. Figure 23 shows the milled flange profile. The circular cut-out on the vertical triangular plate was produced by vertical drilling using a standard twist drill in two stages: a pilot hole to establish accurate centring and reduce thrust force on the full-diameter drill, followed by the finish bore at the specified diameter. Figure 24 shows the circular profile and Figure 25 presents the completed optimised bracket after all machining operations.

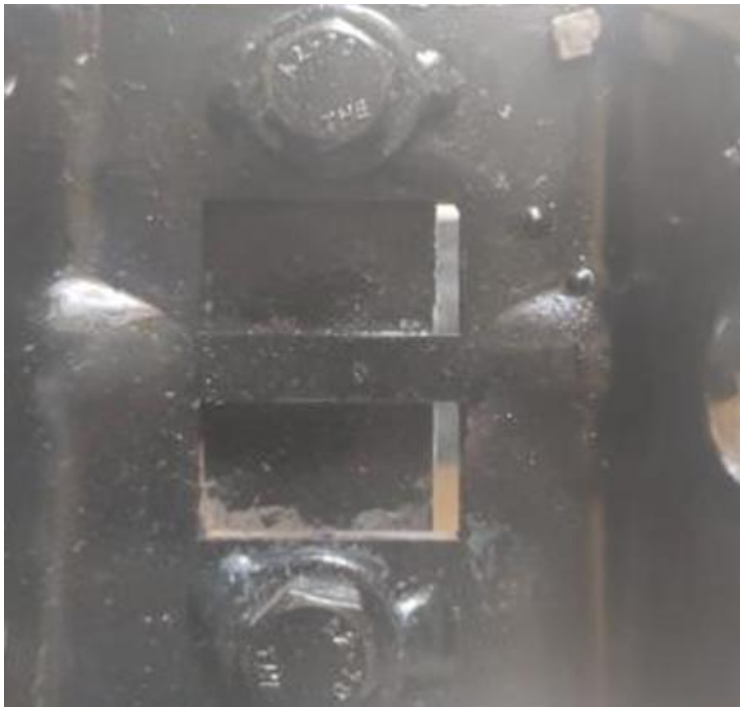

Figure 23. Flange profile produced by vertical CNC milling. The milled surface provides dimensional accuracy and a low surface roughness finish.

Figure 24. Circular cut-out produced by two-stage drilling (pilot hole followed by finish bore) on the vertical triangular plate.

Figure 25. Completed optimised leaf spring bracket following all three machining operations, ready for fixture mounting and strain gauge testing.

6.2 Test Fixture and Strain Gauge Instrumentation

A purpose-built test fixture was fabricated from C-channel structural steel sections to replicate the chassis frame boundary conditions during laboratory testing. The bracket was attached using five high-strength bolts replicating the five-bolt chassis attachment configuration, and a freely rotating cylindrical loading pin was inserted through the central bore to transmit the UTM actuator load in the same manner as the leaf spring mounting pin in the vehicle. Rotation freedom of the pin prevented the introduction of parasitic bending moments at the load application point. Figure 26 shows the bracket mounted on the test fixture.

Strain measurement was performed using uniaxial foil resistance strain gauges bonded to the bracket surface using cyanoacrylate adhesive following thorough surface preparation (degreasing, abrasion, and re-cleaning). The gauge output was acquired by a Wheatstone bridge circuit and digital data logger, with strain computed from the measured resistance change as $\varepsilon = (\Delta R/R)/GF$, where GF is the manufacturer-specified gauge factor. The gauge was positioned on the flat surface of the horizontal plate in the region of highest accessible strain, consistent with the FEA strain distribution. Figures 27 show the gauge specifications, load application setup, and gauge mounting location respectively.

Figure 26. Optimised bracket assembled on the fabricated C-channel test fixture, secured with five high-strength bolts at the chassis attachment positions.

6.3 Test Results and FEA Correlation

The vertical load was applied quasi-statically in incremental steps from 0 to 6,000 N, with strain gauge readings recorded at each increment. The measured strain at 6,000 N was 153.2 microstrain, corresponding to a computed stress of $\sigma = E\varepsilon = 210{,}000 \times 153.2 \times 10^{-6} = 32.2$ MPa, confirming that the bracket operates well within the elastic regime (yield strength 340 MPa). Figure 27 presents the experimental load-strain relationship, which is linear throughout the loading range, consistent with purely elastic material response.

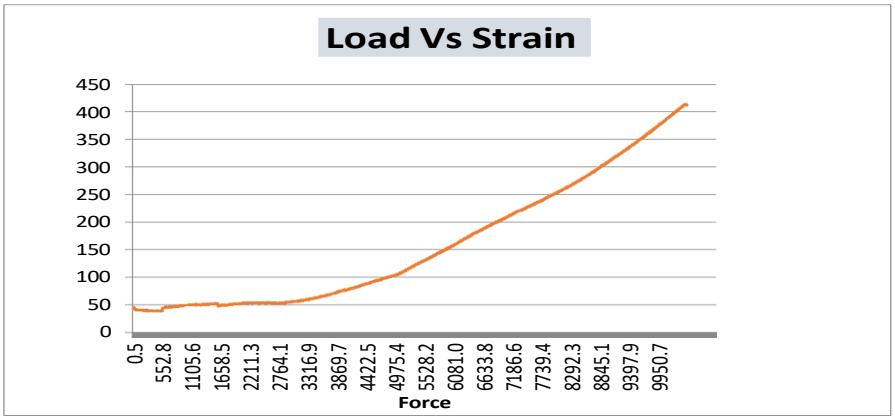

Figure 30. Experimentally measured load versus strain at the gauge location. The linear relationship confirms elastic behaviour throughout the 0–6,000 N loading range.

The FEA-predicted strain at the gauge node under the same loading was 180.7 microstrain. The resulting discrepancy of 15.2 percent is within the accepted range for structural correlation testing of fabricated metallic components. Known sources of systematic discrepancy include dimensional tolerances on the machined cut-out profiles, gauge placement offset from the FEA node, adhesive layer compliance, and the rigid-weld assumption in the FEA model (which slightly overstates weld zone stiffness and consequently overpredicts local strain). The direction of discrepancy FEA exceeding experimental is consistent with the well-documented conservative tendency of linear elastic FEA to slightly overestimate strains in regions adjacent to geometric discontinuities. Figure 28 superimposes both load-strain curves and confirms that the two datasets are in close agreement across the full loading range.

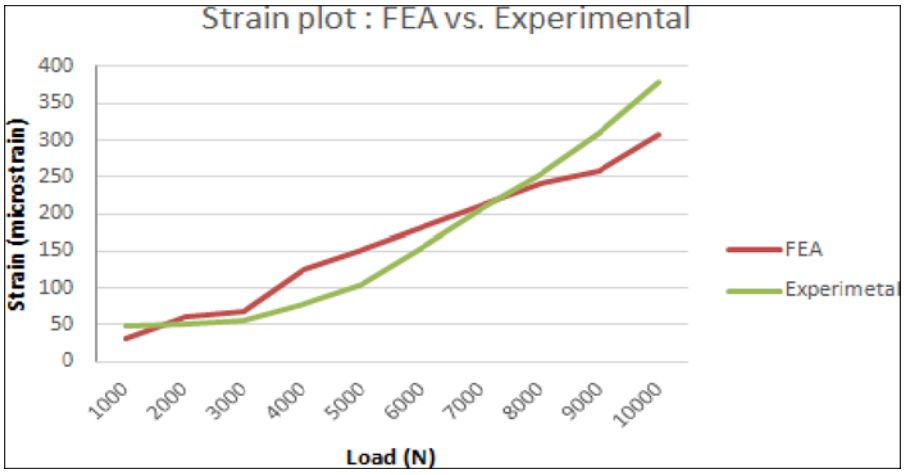

Figure 31. Comparative load versus strain curves from experimental strain gauge testing and FEA prediction. Parallel linear trajectories confirm that the FEA model correctly captures bracket stiffness, with a systematic 15.2 percent offset attributable to manufacturing tolerances and modelling assumptions.

7. Results And Discussion

7.1 Comparative FEA Performance

Table 3 consolidates the FEA structural performance metrics for the original and optimised bracket designs under the 6,000 N service load. The results confirm that the topology optimisation exercise delivered a 200 g (11.1 percent) mass reduction while preserving or marginally improving all structural performance indicators.

Table 3. Comparative FEA performance metrics: original bracket versus topology-optimised bracket at 6,000 N applied load.

Performance Parameter	Original Bracket	Optimised Bracket	Change
Maximum Deformation	0.130 mm	0.125 mm	−3.8%
Peak Equiv. von Mises Stress	67.90 MPa	66.79 MPa	−1.6%
Maximum Equiv. Strain	5.36×10^{-4} m/m	4.95×10^{-4} m/m	−7.6%
Minimum Fatigue Life	Infinite (>10^6 cycles)	Infinite (>10^6 cycles)	No change
Min. Fatigue Factor of Safety	2.018	2.020	+0.1%
Component Mass	1.800 kg	1.600 kg	−11.1%

Figure 32. Visual comparison: (a) original leaf spring bracket, (b) topology-optimised bracket with rectangular horizontal slot and circular vertical cut-out. The two geometric modifications are clearly visible.

Several features of the comparative results merit detailed discussion. The marginal reduction in both peak stress and maximum deformation in the optimised design despite material removal is a characteristic outcome of compliance minimisation topology optimisation. The SIMP algorithm drives material towards the primary load path and away from low-stress regions. Removing material from zones that were not carrying significant load does not increase the stress in the retained material; on the contrary, the slight redistribution of

the effective stiffness distribution towards higher-efficiency load-transfer paths can marginally reduce peak stress in the critical zones [7,8]. This behaviour distinguishes topology-optimised weight reduction from simple geometric cutback, which would typically increase peak stress.

The preservation of infinite fatigue life and an essentially unchanged minimum fatigue factor of safety (2.018 to 2.020) demonstrates that the material removed by the optimisation was exclusively located in regions whose fatigue factor of safety substantially exceeded the 2.0 threshold. The topology optimisation mass retention constraint was formulated at the global level (80 percent of total mass retained), which does not guarantee that no critical zone is inadvertently compromised. The fact that the minimum factor of safety was maintained confirms that the algorithm correctly identified the critical load path and preserved the associated material.

7.2 Experimental Validation Assessment

Table 4. Quantitative comparison of FEA-predicted and experimentally measured strains at the gauge location on the optimised bracket under 6,000 N.

Test Configuration	FEA Strain (με)	Experimental Strain (με)	Discrepancy
Optimised bracket at 6,000 N	180.7	153.2	15.2%

The 15.2 percent discrepancy between the FEA prediction and experimental measurement is within the range documented in comparable structural validation programmes for welded and machined steel components [3,4,5]. The linear load-strain behaviour observed throughout the 0–6,000 N loading range provides independent confirmation of the elastic response assumption underpinning the linear static FEA model. The consistent overestimation of strain by FEA is of the correct sign and magnitude to be explained by conservative modelling assumptions (rigid weld) combined with normal manufacturing variability, and does not indicate a systematic modelling error.

The achieved 11.1 percent mass reduction is somewhat below the 20 percent target set by the topology optimisation mass retention constraint. This shortfall is inherent to the interpretation phase: the SIMP algorithm produces a continuous density field that, in regions of intermediate density, prescribes partial material retention. Translating this output into manufacturable binary features (material present or absent) invariably retains some material that the algorithm identified as redundant but which cannot be removed as a geometrically coherent feature within the constraints of available subtractive machining processes. This limitation is well recognised in the literature [2,5] and motivates the integration of topology optimisation with additive manufacturing processes in future work.

8. CONCLUSIONS

The following principal conclusions are drawn from this investigation:

(1) Topology optimisation implemented within ANSYS Workbench 19 using the compliance minimisation objective and an 80 percent mass retention constraint provided a rigorous, quantitative basis for material removal decisions in the leaf spring mounting bracket of a light commercial diesel truck, replacing designer intuition with an algorithmic load-path identification procedure.

(2) The re-engineered optimised bracket achieved a mass reduction of 200 grams (11.1 percent, from 1.800 kg to 1.600 kg) through the introduction of a rectangular slot on the horizontal plate and a circular cut-out on the vertical triangular plate, without any change in material grade or manufacturing process class.

(3) Peak equivalent von Mises stress decreased marginally from 67.9 MPa to 66.79 MPa (−1.6%), and maximum deformation decreased from 0.130 mm to 0.125 mm (−3.8%). Both values remain well below the material yield strength (340 MPa) and endurance limit (170 MPa) respectively, confirming full structural equivalence.

(4) Both the original and optimised designs exhibit infinite fatigue life under the design service load, with essentially identical minimum fatigue factors of safety (2.018 and 2.020 respectively), demonstrating that the topology optimisation successfully isolated and removed structurally redundant material without encroaching on the critical fatigue zones.

(5) A shape optimisation study confirmed the circular cut-out as the most suitable vertical plate geometry: all three candidate shapes (square, circular, triangular) produced equivalent global stress levels, but the circular profile uniquely eliminates corner stress concentrations, which would otherwise constitute potential fatigue crack initiation sites under cyclic service loading.

(6) Experimental strain gauge testing yielded 153.2 microstrain at 6,000 N, against an FEA prediction of 180.7 microstrain, a 15.2 percent discrepancy within accepted validation tolerance. The linear load-strain behaviour observed experimentally confirms that the bracket operates in the elastic regime and validates the linear FEA model as a reliable predictor of bracket structural behaviour.

REFERENCES

[1] J. W. Chang and Y. S. Lee, 'Topology optimisation of compressor bracket,' Journal of Mechanical Science and Technology, vol. 22, pp. 1668–1676, 2018.

[2] G. Chiandussi, I. Gaviglio, and A. Ibba, 'Topology optimisation of an automotive component without final volume constraint specification,' Advances in Engineering Software, vol. 35, pp. 609–617, 2004.

[3] V. Neelakandan, T. Ganaeshan, and P. Rao, 'Weight optimisation of housing bracket for electrical starter motor using FEA,' International Journal of Engineering Research and Technology, vol. 3, no. 7, 2014.

[4] Vhanshetti and N. S. Chavan, 'Design of integrated super bracket for heavy commercial vehicles,' International Journal of Advanced Engineering Research and Science, vol. 2, no. 1, pp. 1–7, 2015.

[5] S. G. Barbieri, M. Giacopini, V. Mangeruga, and S. Mantovani, 'A design strategy based on topology optimisation techniques for an additive manufactured high performance engine piston,' Procedia Manufacturing, vol. 11, pp. 641–649, 2017.

[6] P. Wu, Q. Ma, Y. Luo, and C. Tao, 'Topology optimisation design of automotive engine bracket,' Energy and Power Engineering, vol. 8, pp. 230–235, 2016.

[7] G. H. Gowd and E. V. Goud, 'Static analysis of leaf spring,' International Journal of Engineering Science and Technology, vol. 4, no. 8, pp. 3794–3799, 2012.

[8] R. Prakash, V. Kavinraj, A. Anandajayakumar, and S. Karthik, 'Design and analysis of leaf spring bracket in air suspension vehicle using FEA,' International Journal of Engineering Research and Technology, vol. 3, no. 5, 2014.

[9] C. Radhakrishnan, K. Azhagendran, K. Mohanlal, P. Ponraj, and R. Nivas, 'Design and analysis of automotive shackle,' International Journal of Innovative Science, Engineering and Technology, vol. 2, no. 5, 2015.

[10] M. Dasgaonkar, A. Hambar, and P. Baskar, 'Design optimisation and analysis of leaf spring using static load conditions,' International Journal for Research in Applied Science and Engineering Technology, vol. 4, no. VII, 2016.

[11] R. Browell and A. Hancq, Calculating and Displaying Fatigue Results. ANSYS Technical Publication, 2006.

[12] M. Dhaytonde, K. Kolhapure, and V. Chahare, 'Design analysis of structural steel and carbon fiber leaf spring,' International Journal of Research in Aeronautical and Mechanical Engineering, vol. 12, no. 10, pp. 1–15, 2024.

[13] B. Gibbs, N. A. Alsaleh, A. Abdelwahab, F. Hafeez, S. Ataya, and K. Essa, 'The performance of a concept 3D printed carbon fibre-reinforced polymer mono-parabolic leaf spring,' International Journal of Advanced Manufacturing Technology, 2025. doi:10.1007/s00170-025-17018-0

[14] M. I. Khan and K. Kolhapure, 'Weight optimization of leaf spring assembly using design for manufacturing approach and FEM in graduated leaves for electric vehicle,' International Journal of Applied Mechanics and Engineering, vol. 30, no. 1, pp. 89–100, 2024.

[15] W. Krason, P. Bogusz, and J. Wysocki, 'Research on the influence of the mounting configuration on the elastic characteristics and energy dissipation capacity of multi-leaf springs for truck vehicles,' Energies, vol. 17, no. 22, p. 5688, 2024.

[16] J. Wang, N. Wei, and Q. Xu, 'Research on mechanical performance analysis and topology optimization design of new automobile frame structures,' Journal of Engineering Mechanics and Machinery, vol. 9, no. 3, pp. 15–22, 2024.

[17] B. A. Tadesse and O. Fatoba, 'Design optimization and numerical analyses of composite leaf spring in a heavy-duty truck vehicle,' Materials Today: Proceedings, vol. 62, no. 6, pp. 2814–2821, 2022.

[18] P. D. Borase, G. K. Khare, and V. Babele, 'A review of stress analysis and advanced FEA techniques in automotive suspension systems,' International Journal of Scientific Research in Engineering and Management, vol. 8, no. 7, pp. 1–11, 2024.

[19] H. H. Khaleel, A. Al Sahlani, N. H. Dhaher, and N. M. Baqer, 'Modeling and analysis of leaf spring using finite elements method,' International Journal of Mechanical Engineering and Technology, vol. 9, no. 6, pp. 48–56, 2018.

[20] C. Li, J. Zou, B. Li, Y. Lei, and M. Zhang, 'Lightweight design of front axle structure of a certain type of automobile,' Mechanical Engineering Science, vol. 7, no. 1, pp. 26–32, 2025.